Article

Not peer-reviewed version

AI Driven Modelling for Hydrogel 3D-Printing: Computational and Experimental Cases of Study

Harbil Bediaga-Bañeres , Isabel Moreno-Benítez * , Sonia Arrasate , Leyre Pérez-Álvarez , Amit K. Halder , M. Natalia D. S. Cordeiro , Humberto González-Díaz , José Luis Vilas-Vilela *

Posted Date: 21 November 2024

doi: 10.20944/preprints202411.1644.v1

Keywords: Machine Learning, Artificial intelligence, Database, Hydrogel, Modelling, Bioprinting

Article

AI Driven Modelling for Hydrogel 3D-Printing: Computational and Experimental Cases of Study

Harbil Bediaga-Bañeres [1], Isabel Moreno-Benítez [2,*], Sonia Arrasate [2], Leyre Pérez-Álvarez [1,3], Amit K. Halder [4], M. Natalia D. S. Cordeiro [4], Humberto González-Díaz [2,5,6] and José Luis Vilas-Vilela [1,3,*]

[1] Department of Physical Chemistry, University of Basque Country UPV/EHU, 48940, Leioa, Spain
[2] Department of Organic and Inorganic Chemistry, University of Basque Country UPV/EHU, 48940, Leioa, Spain
[3] BCMaterials, Basque Center for Materials, Applications and Nanostructures, UPV/EHU Science Park, 48940 Leioa, Spain
[4] LAQV-REQUIMTE/Department of Chemistry and Biochemistry, Faculty of Sciences, University of Porto, 4169-007 Porto, Portugal
[5] Basque Center for Biophysics, CSIC-UPV/EHU, 48940, Leioa, Spain
[6] IKERBASQUE, Basque Foundation for Science, 48011, Bilbao, Spain
* Correspondence: mariaisabel.moreno@ehu.eus (I.M.-B.); joseluis.vilas@ehu.eus (J.L.V.-V.)

Abstract: Determining the values of various properties for new bioinks for 3D printing is a very important task in the design of new materials. For this purpose, a large number of experimental works have been consulted and a database with >1200 bioprinting tests has been created. These tests cover different combinations of conditions in terms of print pressure, temperature, and needle values, for example. These data are difficult to deal with in terms of determining combinations of conditions to optimize the tests and to analyze new options. The best model presented has values of specificity = Sp (%) = 88.4, sensitivity = Sn (%) = 86.2 in training series and Sp (%) = 85.9, Sn (%) = 80.3 in external validation series. This model uses operators based on perturbation theory in order to analyze the complexity of the data. The performance of the model has been compared with neural networks with very similar results. This tool could be easily applied to predict the properties of in silico bioprinting assays.

Keywords: machine learning; artificial intelligence; database; hydrogel; modelling; bioprinting

1. Introduction

3D bioprinting has revolutionized tissue engineering and regenerative medicine. This groundbreaking technique involves the manufacture of biologically functional structures using so-called bioinks that contain cells, growth factors or biomaterials. Hydrogels are three-dimensional cross-linked polymeric networks [1] and represent one of the most common components of bioinks, providing structural integrity to the printed tissues [2]. Hydrogels owe their unique suitability as a bioink carrier to special properties such as biocompatibility [3], water content, and the possibility of adjusting mechanical and biochemical properties. Examples of commonly used hydrogels in application are alginate [4], collagen [5], and hyaluronic acid [6] among natural materials, and synthetic polymers like polyethylene glycol [7].

Hydrogel bioinks are normally categorized based on the type of solvent in which they are dissolved since this dictates their composition and functional properties. The two main categories of hydrogel bioinks include water-based hydrogels and polymer blends with organic solvents [8]. Water-based hydrogels are primarily polymeric networks that swell in water, emulating certain characteristics of the natural extracellular matrix [9]. This structure promotes cell adhesion and proliferation; therefore, they are especially suitable in soft tissue engineering applications where

 doi:10.20944/preprints202411.1644.v1

nutrient diffusion and waste removal of cellular debris have to take place. Among them, hydrogels from natural polymers such as alginate, collagen, and gelatin resemble the extracellular matrix (ECM) both chemically and structurally; hence, they are more biocompatible.

In contrast, hydrogels based on synthetic polymers, like Pluronic F127 [10] or polyvinyl alcohol [11], are advantageous in terms of the reproducibility and controllable nature of their physical and chemical properties, which further allows their modification to suit particular applications. On the other hand, organic solvent-based polymer blends are water-insoluble polymers dissolved in solvents such as acetone or dichloromethane; in such applications, after printing, the evaporation rate of the solvent is very high to leave a solid structure [12]. A typical example of this type is FDA-approved polycaprolactone (PCL), used in the impression of bone structure for its excellent biocompatibility with strength and controlled rate of biodegradation [13].

In this context, printability is needed for the accurate fabrication of complex tissues and organs, which is the success of a material in prevailing processes [14,15]. The properties that vary for the high-quality printability of one hydrogel include extrudability, interlayer adhesion, resolution, shape retention, and crosslinking control. Although there are many advancements, research is further needed for complete perfection in some areas [2,16]. One of the major challenges within bioinks is that the majority of them do not meet expectations concerning mechanical strength. Such weakness is related to the complex factors like rheology, cross-linking, and other properties such as viscosity **[17,18]**. To solve the latter problems, a variety of properties and conditions should be considered, such as temperature and concentration of the bioink upon printing. Extrusion is one of the most used printing methods for hydrogels because it is precise, controlled, and compatible with biomaterials [19]. With the continuous progress that is happening in 3D bioprinting, research efforts are bound to be made to overcome some of the current limitations to make hydrogels more relevant in tissue engineering. Challenges involve a very high resolution with increased geometric complexity [20]. Further, there is still much apprehension about the mechanical strength, including the compressive and tensile properties [16]. In addition, various features of hydrogels and mechanical robustness give rise to further complications. These are the challenges that the development of 3D printing with hydrogels has to surmount, considering the types of materials (biopolymers, synthetic polymers, nanocomposites), new technologies such as 4D printing, and their applications in biomedical and bioengineering fields [21].

Indeed, some studies have correlated the bioprinting parameters with the mechanical properties of the obtained hydrogel structures: cartridge temperature [22], bed temperature [23], printing speed [24], extrusion pressure [25], number of printed layers [26], flow rate [27], and cross-linking methods [28].

Artificial Intelligence (AI) and Machine Learning (ML) are fields that focus on the creation of algorithms, which confer computers with capabilities for learning from data in order to improve their performance in specific tasks without explicit programming [29]. The variety of areas these technologies applied to is great: medicine [30], pharmacology **[31–36]**, speech recognition [37], agriculture [38], and computer vision [39]. Given this, AI/AA [40] can automate the construction of analytical models using identification patterns in data to make decisions with limited human intervention in 3D bioprinting [20]. Earlier works, such as those by *Madadian* et al., identified that DoE combined with machine learning provides a superior understanding of 3D printing hydrogels prepared by pneumatic semi-solid extrusion-a technique based on the compression of materials by pressurized air and their extrusion under variable conditions [41]. Particularly, this methodology was useful for the fabrication of pharmaceutical and biomedical products since it allowed their combination with hydrogels containing drugs or cells.

Li et al. described another approach using a chemical library from components capable of forming hydrogels by means of a four-component Ugi reaction [42]. Characterization of the hydrogels was done using a rheometer and a Transmission Electron Microscopy (TEM); after that, they were cultured with an adherent cell line. The team employed machine learning to identify the chemical parameters of the library and map relationships of structure and gelation property [43]. Such research is a breakthrough in optimizing parameters for 3D printing of hydrogels.

 doi:10.20944/preprints202411.1644.v1

Yadav et al. have studied the effects of extrusion temperature, fill density and material density on the mechanical properties of both single and multi-material printed parts. Their experimental results clearly show an interesting relationship between extrusion temperature, filler density, and tensile strength of the parts giving important insights into how the mechanical properties of 3D printed products may be optimized [44].

Although ML has managed to prove that its contribution in big data analysis is a game-changer, just a limited number of works aimed so far at the exploitation of its potential in biomaterial development for 3D printing applications. Among the first applications in this area, *Elbadawi* et al. [45] resorted to ML algorithms in predicting the printability of polymeric filaments in drug delivery by using fused deposition modelling. However, in their study, printability is defined as the ability to extrude from the nozzle without any requirement to form a three-dimensional structure. In biomedical applications, however, shape fidelity is of most importance since this directly affects integration and functionality of the printed product. Such pioneering work has also been done by *Nadernezhad and Groll* [46] using the Random Forest algorithm to predict printability from rheological properties, hence providing some general understanding of how rheology affects printability. However, this study has major limitations: in using only one ML algorithm while data is restricted to a single hydrogel, namely hyaluronic acid, and it relies on rheological tests, which very often need a complex empirical process for predicting printability.

Chen et al. [47] concluded that the use of ML in the prediction of formulations of printable bioinks for three-dimensional structures can systematically guide biomaterials development through accurate classification of formulations, thus identifying printability windows that improve the accuracy of shape fidelity prediction and ultimately the biomedical area where such materials can be applied.

There is no predefined minimum of data to train a predictive model, but the larger the dataset, the more refined the model and better the analyses of the relationships among the variables. In case there was no previous database, Information Fusion (IF) methods can be applied data from several studies or databases may be integrated to create a more complete dataset [48]. This fusion aims to interactively consider all available information in order to get a wider and more detailed overview of the problem. Lastly, Perturbation Theory (PT) operators are mathematical tools that enable one to calculate properties and behavior of a system beyond simple models [49]. IF, PT, and machine learning integration is one of the effective strategies for the challenge of materials design; it has gained successful applications in medicinal chemistry, proteomics, nanotechnology, especially in handling volume data with Big Data characteristics [32,34–36,48–56].

In this study, a versatile IFPTML model for predicting 3D bioprinted scaffold properties based on monomer structure is described. This application of AI/ML in 3D printing aims to enhance the optimization of crucial processes, materials, and printing parameters [57]. These algorithms streamline optimization, enable real-time error detection and reduce the number of iterative steps required for bioink formulation. To achieve this, a database of experimental values documented in the literature was compiled. Various AI/ML-based models were trained to forecast upcoming bioprinting experiments and aid in the design of innovative monomers. All the trained models in this work are available in the repository: https://github.com/hbediaga/hydrogel.git.

2. Materials and Methods

2.1. Computational Methods

2.1.1. Database Creation

The models trained in this study are based on a database created from scratch by combining experimental data obtained by some members of our research group with data obtained from the literature (see Table 1) [58–68]. The bioprinting parameter data obtained consists of one or two hydrogels for each scaffold. The final database includes 1568 assays examining the bioprinting of 10 different hydrogels under wide range of compositions and printing condition. In these studies, 16 different properties were analyzed, including uniformity, porosity, printability, viscosity, width, and

 doi:10.20944/preprints202411.1644.v1

diameter among others. These properties have been unified using methodologies based on IF. The information obtained from the literature have been grouped depending on the conditions used for printing and the measured property of the bioprinted scaffold. To create a consolidated model, the results were categorized into two classes: Good (1) and Poor (0). In this way the data could be analyzed comprehensively, enabling a multi-property model to be developed. The result of each assay was expressed by one experimental parameter v_{ij} used to quantify the physicochemical properties of the ith hydrogel (m_i) over the jth target. The values of v_{ij} depend on the structure of the hydrogel and on a series of boundary/experimental conditions that delimit the characteristics of the assay $c_j = (c_0, c_1, c_2, \ldots c_n)$. The first c_j was c_0 = the measured property (porosity, uniformity, etc.) per se. Other conditions are c_1 = Extrusion Pressure (kPa), c_2 = Extrusion speed (mm/s), c_3 = Nozzle, c_4 = Nozzle inner diameter (μm), c_5 = Layers printed, c_6 = Mixture temperature (ºC), c_7 = Syringe temperature (ºC), c_8 = Platform temperature (ºC) and c_9 = Ethanol content (Yes or No). Considering that, in many cases, the compiled values v_{ij} are not exact numbers, classification techniques were used instead of regression methods and de values were discretized as: $f(v_{ij})_{obs} = 1$ when v_{ij} > cut-off.

2.1.2. Descriptors Calculation

In addition to the experimental data previously described, the database was completed with the values of the molecular descriptors that serve as the foundation for converting categorical variables into numerical ones. To obtain the values of these molecular descriptors, the SMILES code [71] of the monomeric unit that form the hydrogel polymer was employed. The Python [72] libraries Mordred [73] and alvaDesc [74] from the OCHEM website (https://ochem.eu/home/show.do) were used to extract these molecular descriptor values. Both options are available free of charge. In the case where the bioink was composed of two hydrogels, the values of the descriptors are added as a proportion of the concentration of each one.

Table 1. Bibliography used for the creation of the database and detailed summary of the selected compounds.

Author	HA[a]	ChiMA[b]	Gelatin	Alginate	MC[c]	Agarose	NOOC[d]	GelMA[e]	GG[f]	Chitosan	Ref.
Aguado et al.				x							[58]
Almeida et al.										x	[59]
Butler et al.						x	x				[60]
Chen et al.				x					x		[61]
Di Giuseppe et al.			x	x							[65]
Firipis et al.				x		x					[63]
Gao et al.			x	x							[69]
Jain et al.								x			[66]
Maíz-Fernandez et al.	x	x									[68]
Negrini et al.					x						[62]
Ouyang et al.			x	x							[67]
Soltan et al.			x	x							[70]

[a] Hyaluronic Acid; [b] Chitosan Methacryloyl; [c] Methyl Cellulose; [d] N,O-carboxymethyl chitosan; [e] Methacrylated Gelatin; [f] Gellan Gum.

2.1.3. Outcome Classification

As previously commented, the database comprises measurements of 16 properties associated with the printability of hydrogels. Given the considerable number of properties intended for analysis, the results were classified into two categories. On the one hand, experiments with property values close to the desired value or the average of experiments (in cases where no specific desired value was

 doi:10.20944/preprints202411.1644.v1

available) are designated as '1'. On the other hand, experiments with results that do not meet the desired criteria, whether above or below the established limits, are classified as '0'. To establish these thresholds, a search for a range that would allow experiments to be classified as '1' was conducted, ensuring a representative number of cases in both cases and a balance between them. This process starts with the average or desired value, tallying the data in each group with varying deviations. The optimal classification was derived from the classification thresholds or cut-offs presented in Table 2.

2.1.4. Model Generation Process

PTML modeling technique is useful for seeking predictive models for complex datasets with multiple Big Data features. Scoring function values $f(v_{ij})_{calc}$ for the ith hydrogel in the jth process conditions with multiple condition of assay $c_j = (c_0, c_1, c_2, \ldots c_n)$ can be predicted. PT operators similar to Box-Jenkins Moving Averages (MA) [75] operators $\Delta D_k(c_j)$ are used as input [76] for the kth descriptor. The development of linear IFPTML models holds immense promise in the field of 3D bioprinting. These models offer a structured and interpretable approach for prediction printability properties and classifying compounds. By integrating data from various sources, these models can effectively capture the relationships among monomer structures, printing parameters, and printability outcomes.

Table 2. Summary of results, including ranges of values (minimum, maximum, average) and distribution of rankings (n_0 and n_1) for each possible outcome.

Outcome (Unit)	Lim. Inf.	Avg	Lim. Supp.	n_0	n_1	Ref.
Uniformity, U	0.93	0.98	1.03	62	36	[68–70]
Pore factor, Pr	0.90	0.95	1.00	28	11	[14,63,66,67, 70]
Integrity factor, I	0.30	0.61	0.70	16	13	[69,70]
Viscosity (cP)	1800.00	3054.86	15000.00	10	4	[58,70]
Accuracy, Ac	82.82	87.18	91.54	12	3	[65]
Width	0.32	0.33	0.35	3	3	29h
Parameter Optimzation Index, POI	40.00	57.04	65.00	3	3	29h
Compr. Modulus (kPa)	35.00	38.13	42.00	3	3	29h
Storage, G′	25.00	468.10	95.00	12	7	[58,60,69]
Loss moduli, G″	0.40	0.75	0.85	5	1	[60]
tan(G″/G′)	0.20	0.32	0.40	6	4	[69,70]
Swelling ratio, Sw	10.71	11.28	11.84	2	2	[61]
E (Pa)	100.00	830.99	2000.00	2	4	[69]
Diameter (mm)	100.00	735.44	772.21	18	30	[62]
Porosity (%)	78.00	77.35	85.00	1	1	[59]
Expansion (%)	8.00	10.18	25.00	628	632	[68]
Total				811	757	

IFPTML models allow researchers to understand the underlying factors influencing printability. This transparency is crucial for refining and optimizing the bioprinting process. Structural features of monomers with a most significant influence on printability can be detected, allowing the proposal of specific modifications and design improvements.

IFPTML model starts with the expected value of a printing property and adds the effect of different perturbations in the system. Consequently, the model has two types of input variables: the expected-value function $f(v_{ij})_{expt}$ and the PT operators $D_k(c_j)$. The input variable $f(v_{ij})_{expt}$ represents the expected value of the printing property for hydrogel in different combinations of printing conditions $c_j = (c_0, c_1, c_2, \ldots c_j \ldots c_{max})$. The other PT operators are MA calculated for one condition at time. So, PT

 doi:10.20944/preprints202411.1644.v1

operators can be calculated as follows: $D_k(c_j) = D_{ki} - \langle D_k(c_j) \rangle$. The operators depend on the value of the molecular descriptor D_{ki} of type k used to quantify the structure of the ith monomer. The PT operators measure the deviation of D_{ki} from the expected value of $\langle D_k(c_j) \rangle$ (average value) of this descriptor for different sets of monomers c_j. The output of the model $f(v_{ij})_{calc}$ is a scoring function of the value v_{ij} of printing property of the ith monomer in the different combinations of the conditions of the assay c_j. See Supporting Information file S1.xlsx for database.

3. Experimental Methods

3.1. Bioprinting Conditions

Separate solutions of methacrylated Chitosan (ChiMA, 1.5% (w/w)) dissolved in 0.5% (v/v) acetic acid and polyethylene glycol diacrylate (PEGDA, 20 mM) were prepared. Then, a solution of PEGDA was added to CHIMA solution and stirred for 24 hours. The photoinitiator lithium phenyl-2,4,6-trimethylbenzoylphosphinate (LAP, 0.1% (w/w)) previously dissolved in 300 µL of 0.5% (v/v) acetic acid solution was added.

A bioprinter (INKREDIBLE + Cellink) was used to print the hydrogels scaffolds, which were previously prepared and loaded into a cartridge (Adhesive Dispensing Ltd.). Hydrogel scaffolds were printed with a cell side length of 5 mm, at a speed of 600 mm/min, with a nozzle inner diameter of 0.254 mm and a pressure of 21-27kPa. Subsequently, the hydrogel grid was photopolymerized in situ with an ultraviolet light LED (405 nm, 19 mW/cm2) [68].

3.2. Image Caption and Analysis

The grid was analyzed with an optical magnifying glass (Nikon AZ100 Multizoom) where photos were taken at one and two magnifications. With the ImageJ software, the impression of the hydrogel lines was analyzed. In particular the expansion ratio and the uniformity factor were calculated [77].

4. Results and Discussion

4.1. Computational Model

Python (3.9.11) code has been developed to process the data and generate the models to be presented in this section. The best results obtained for each type of model are shown. These models can be used to score the properties of a new hydrogel in different combinations of conditions of assay. Firstly, we have to substitute the reference function value must be substituted in the selected equation. It is noteworthy that these values change for different properties. Consequently, the model can predict different kinds of property parameters for a single hydrogel. Subsequently, the descriptors' values for a new hydrogel must be input into the model. These values were determined using various calculation methods. In order to calculate these expected values of probability we have to evaluate the formula $p(f(v_{ij})_{obs} = 1)_{expt} = n(f(v_{ij})=1)_{obs/nj.}$ This ratio was computed by dividing the number of monomers, denoted as $n(f(v_{ij}) = 1)_{obs}$, that satisfy the specified ratio for condition c_j, by the total number of compounds, n_j, tested under the same condition c_j. The models presented are all based on the IFPTML process explained in the previous section.

4.1.1. IFPTML Linear Model

The Linear Discrimination Analysis (LDA) model is a statistical method for finding a linear combination of attributes or characteristics to separate into groups. In the particular case of a LDA model $f(v_{ij})_{calc}$ is not in the range 0-1 and is not a probability. The effectiveness of this type of models is based on the simplicity of its equations. However, it is important to note that the predictions obtained may not have a high degree of confidence. However, for a given value of $f(v_{ij})_{calc}$ the LDA algorithm can calculate the respective values of posterior probabilities $p(f(v_{ij}) = 1)_{pred}$ [78]. The model has two types of input variables: the expected-value function $f(v_{ij})_{expt}$ and the PT operators $D_k(c_j)$. As mentioned above, the database has many input variables. In order to obtain a model with as few

 doi:10.20944/preprints202411.1644.v1

variables as possible, Recursive Feature Elimination (RFE) selection was carried out [79]. In order to analyze the quality of the model, a bootstrapping with 100 iterations was performed, see Figure 1A. With this method, taking the coefficients of the variables as a characteristic, less important sets are selected and eliminated from the model. This procedure was repeated until a model with 10 variables was obtained. Unfortunately, although this model usually gives good results, in this case, selectivity and specificity parameters were not good (see Table 3).

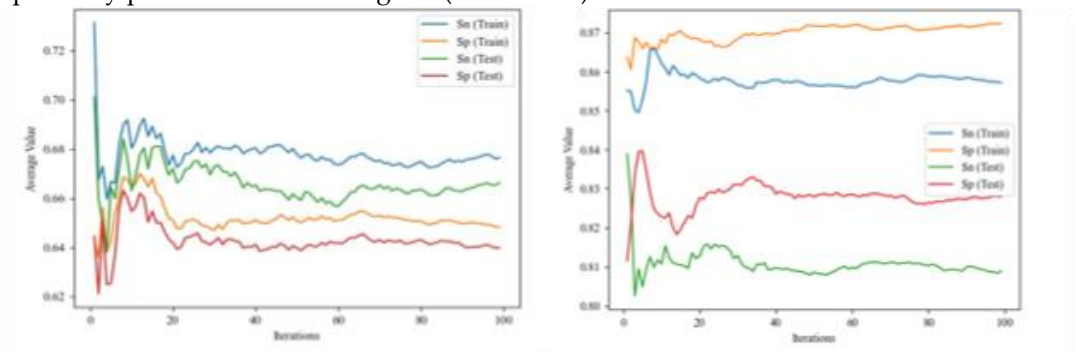

(A) (B)

Figure 1. Comparison of sensitivity (Sn) and specificity (Sp) for the training and validation sets after bootstrapping with increasing training iterations. Subfigure 1A presents the results for the IFPTML-LDA model, while subfigure 1B shows the results for the IFPTML-DTC model.

Table 3. Confusion matrices for the IFPTML-LDA and IFPTML-DTC models, showing the observed and predicted case counts along with the sensitivity (Sn) and specificity (Sp) percentages for each model. The results are organized in the first column, allowing a detailed comparison of the performance parameters between the two models.

Model	**Data Set**	**Classes** $f(v_{i,j})_{obs}$	**Stat.**	**(%)**	n_j	$f(v_{i,j})_{pred}$ **0**	**1**
IFPTML-LDA	training	0	Sp	72.8	558	406	103
		1	Sn	80.9	539	152	436
	validation	0	Sp	71.0	252	179	50
		1	Sn	77.2	219	73	169
	Data Set	Classes $f(v_{i,j})_{obs}$	Stat.	(%)	n_j	$f(v_{i,j})_{pred}$ 0	1
IFPTML-DTC	training	0	Sp	88.4	562	497	74
		1	Sn	86.2	535	65	461
	validation	0	Sp	85.9	248	213	44
		1	Sn	80.3	223	35	179

After evaluating the results obtained with the IFPTML-LDA model, the possibility of improving class differentiation by refining the threshold definition functions was investigated.

4.1.2. IFPTML Non-Linear Models

Finally, some non-linear algorithms were investigated in order to achieve improvements in model performance compared to linear models. On the hand, we trained Decision Tree Classifier (DTC) and different Artificial Neural Network (ANN) models. The IFPTML-DTC model utilizes the framework of a decision tree, employing a flowchart-like structure where decisions are determined at each node based on specific attributes. Upon completion, each branch corresponds to a class, and each path from the root to a final branch defines a classification rule. In this case, as in the linear model, 100 iterations of the model have been analyzed to obtain the best result. The values of the model quality parameters over the iterations can be seen in the Figure 1B and the results of the parameters obtained for the best model can be seen in the Table 3.

 doi:10.20944/preprints202411.1644.v1

Although, this model exhibits commendable performance in relation to the training set, the values for the statistical parameters of the validation set show a slight decrease. This difference in value was not observed in the case of the linear IFPTML-LDA model. As for the values of the parameters themselves, those obtained in the IFPTML-DTC model are much better, and it was mainly for this reason that this model was chosen as the best obtained and used to make the predictions. Nevertheless, all these models are available in the repository for use. The IFPTML-DTC model shown in Table 3 consists of 15 variables and a maximum of 40 leaf-nodes.

The structure of the tree obtained can be seen in Figure 2A. By schematizing and splitting this tree for analysis, we can see 4 main families (Figure 2B). These families are obtained from the first three nodes of the tree. The first family describes 27.8% of the data and arises directly from the main node of the model. The second family (10.6%), the third (40.7%) and the fourth (21.0%) come from the same node.

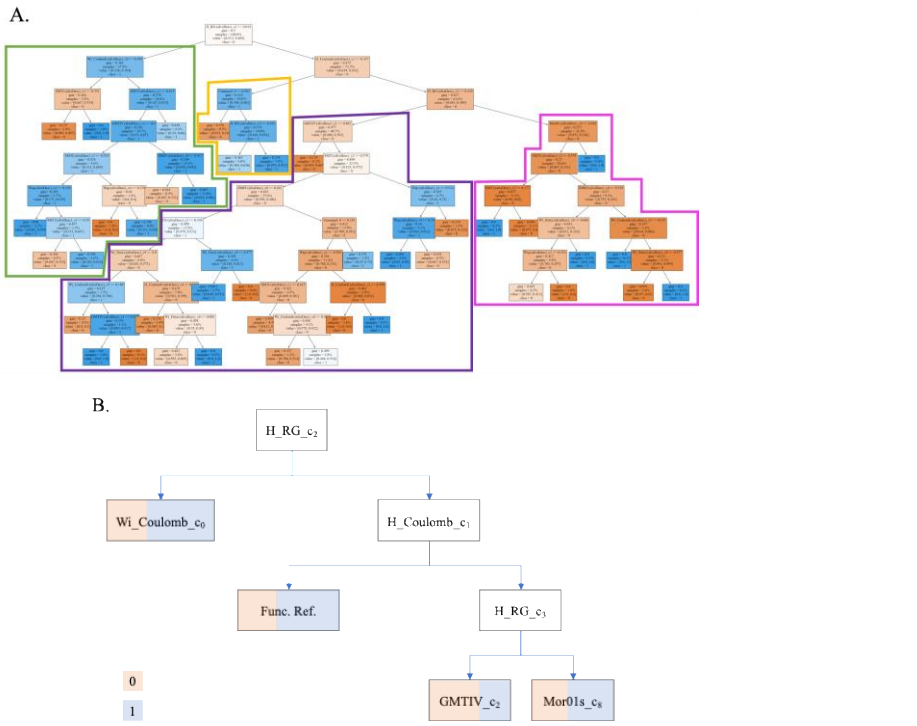

Figure 2. A. Structure of the IFPTML-DTC model, showing all nodes and leaves with indicative classification colors. The branches highlight the different families differentiated in the model. B. Simplified schematic of the main families identified, highlighting the key groupings obtained in the model.

The first family differs from the rest because the hydrogels included on it have a value of the input variable $\Delta HRG(c_2)$ greater than 0.014. This variable is equal to $\Delta HRG(c_2) = HRG_i - \langle HRG(c_2) \rangle$. As you can see in Table 5 the first term of $\Delta HRG(c_2)$ is the index HRG_i of the repetitive unit of the hydrogel. The value HRG_i is the Harary-like index from reciprocal squared geometrical matrix. Then, HRG_i accounts for the number of interactions/contacts between non-bonded atoms. It means that a high HRG_i may indicate that the hydrogel repetitive unit is more compact, or branched (more folded over itself). [80] On the other hand, the second term $\langle HRG(c_2) \rangle$ is the average value of HRG_i (expected value) for all hydrogels measured under the same condition c_2 = extrusion speed. Consequently, the Hydrogels included in this family are those with a deviation greater than 0.014 in the structural branching of the unit with respect those measured at the same extrusion speed and each output properties. This implies that for designing new hydrogels we should carry out a fine tuning of this parameter. The distribution of properties by families can be seen in Figure 3.

Preprints.org (www.preprints.org) | NOT PEER-REVIEWED | Posted: 21 November 2024 doi:10.20944/preprints202411.1644.v1

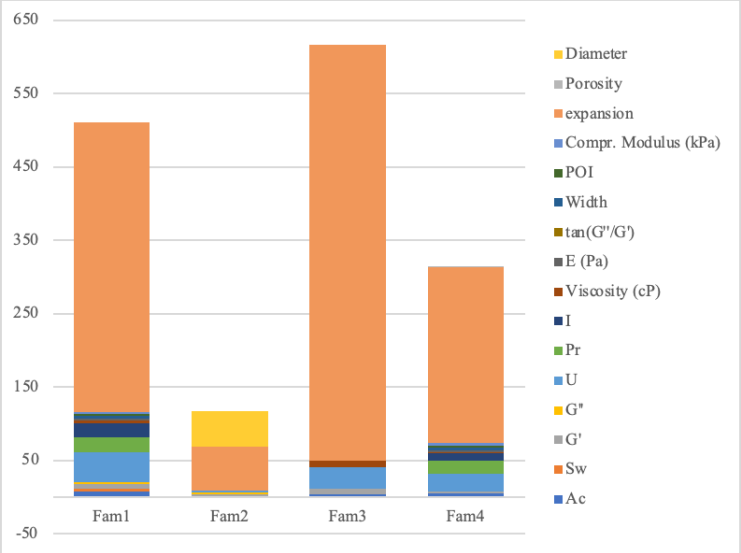

Figure 3. Distribution of the properties measured in each family, showing the variability and range of values observed within each identified group.

By analogy to the first node of the tree, the third family was separated from the second node of the tree by the variable $\Delta HRC(c_1) > 0.357$. These variable measures the deviation of the value of the Harary-like index from Coulomb matrix (HRC) from the expected value for all hydrogels measured under the same extrusion pressure (c_1). With this index global 3D representations of molecular structure and electrostatic interactions among atoms are quantified. So the index is a measure of the branching and electrostatic interactions inside the repetitive units of the hydrogel [81]. This subset representing 10.6% of the data was considered as a family given its short path to the final classification nodes.

Finally, the third node level was analyzed, which creates the separation of the main families or clusters. In this case the cut-off was defined by $\Delta HRG(c_3) > 0.428$. These are deviations of the HRG index of the hydrogel (chemical structure branching) repetitive unit with respect to the average values for all hydrogels measured under the same condition c_3 = Nozzle. The third family emerges as the most complex in terms of the number of nodes on its path and was the family that represents the most points in the database with 17 end nodes. (The IFPTML-DTC model structure can be viewed in supplementary material S2.pdf). Other variables accounting for deviations $\Delta D_k(c_j)$ on structural parameters D_k of the hydrogel under study with respect to the expected/average value for other hydrogels measured under different conditions are used to define subfamilies inside this bigger family. The input variables more commonly used account for deviations $\Delta D_k(c_j)$ with respect to c_1 = extrusion pressure, c_2 = extrusion speed, and c_4 = nozzle inner diameter. However, the deviations with respect to c6 = polymer temperature and c_7 = syringe temperature do not enter the model (see Table 5).

The descriptors used by the model can be seen in Figure 3 and are described in Table 4. This table summarizes the number of times each descriptor appears in the model and the number of the condition to which it was linked to calculate de MA operator. It can be seen that the one that appears most often was the Wiener index, which refers to a topological index of the molecule defined as the sum of the lengths of the shortest paths between all pairs of vertices of the chemical graph representing the non-hydrogen atoms in the molecule [82]. From this index, others have been used to define different ways of calculating the connections between atoms [83]. In the study by Bonchev et al. a mathematical scenario for analyzing the distances between atoms within polymers was analyzed. For this, Wiener indices were used and the relationship of these indices with the branching and the length of the branches was shown. With this index and those defined later, the macroscopic properties of the polymers, in this case hydrogels, can be analyzed qualitatively [84].

 doi:10.20944/preprints202411.1644.v1

Table 4. Descriptors selected in the IFPTML-DTC model, with details of each, including abbreviation, full name, general description of the assessed characteristic, related condition or variable and the frequency with which each descriptor was selected in the model.

Input Variables $\Delta D_k(c_j)$	Descriptor Code	Name	Description	Related Condition (c_j)	Condition name	Nodes Count	Ref.
$\Delta Wap_i(c_4)$	Wap_i	All-path Wiener index	Counts the number of bonds between pairs of atoms to generate a matrix. Does not take hydrogens into account.	4	Nozzle inner diameter	3	[85]
$\Delta Wap_i(c_1)$				1	Extrusion pressure	3	
$\Delta WiDzv_i(c_0)$	$Wi\_Dz(v)_i$	Wiener-like index from Barysz matrix weighted by van der Waals volume		0	Measured property	1	[82]
$\Delta WiDzv_i(c_9)$				9	Ethanol content	4	
$\Delta WiCoulomb_i(c_0)$	$Wi\_Coulomb_i$	Wiener-like index from Coulomb matrix		0	Measured property	2	[86]
$\Delta WiCoulomb_i(c_5)$				5	Layers printed	2	
$\Delta HRG_i(c_3)$	H_RG_i	Harary-like index from reciprocal squared geometrical matrix	It counts the number of bonds of disordered atoms, always taking the shortest path.	3	Nozzle	2	[80,87]
$\Delta HRG_i(c_2)$				2	Extrusion speed	1	
$\Delta HCoulomb_i(c_1)$	$H\_Coulomb_i$	Harary-like index from Coulomb matrix		1	Extrusion pressure	3	
$\Delta HCoulomb_i(c_4)$				4	Nozzle inner diameter	1	
$\Delta Mor01s_i(c_3)$	$Mor01s_i$	Moran autocorrelation of lag 1 weighted by I-state	It is a correlation of two signals between atoms close to each other in space.	3	Nozzle	1	[88]
$\Delta GMTIV_i(c_1)$	$GMTIV_i$	Gutman Molecular Topological Index by valence vertex degrees	A weighted sum that considers the vertices and valences of all pairs of atoms in a graph.	1	Extrusion pressure	2	[83,89]
$\Delta GMTIV_i(c_2)$				2		1	
$\Delta SMTI_i(c_1)$	$SMTI_i$	Schultz Molecular Topological Index		1		4	[74]
$\Delta SMTI_i(c_2)$				2		5	

 doi:10.20944/preprints202411.1644.v1

$\Delta IDMT_i(c_0)$	$IDMT_i$	Total information content on the distance magnitude		0	Measured property	2
	$f(v_{i,j})_{ref}$	Reference function	Value dependent on the property to be calculated.	-		2

In this work, we have also developed three types of supervised learning-based neural networks in addition to linear models to assess which technique has better predictive capability. In addition to linear models, and for comparative purposes, three types of supervised learning-based neural networks were developed. The development of these models was carried out using TensorFlow [90] and Keras [91] libraries. Neural networks with varying degrees of complexity in terms of network type and the number of both hidden layers and neurons have been created. Similar to the previous models, the models that yielded the best results are available in the GitHub repository.

A Multi-Layer Perceptron Classifier (IFPTML-MLPC) is a type of ANN used in machine learning. It consists of multiple layers of dense-interconnected nodes and each layer processes and transforms data through a set of weighted connections. The outcomes of these different complexity IFPTML-MLPC neural networks can be observed in Table 5.

Table 5. Results of IFPTML-DEEP-ANN models trained with different levels of hidden neurons, showing observed versus predicted counts, sensitivity (Sn) and specificity (Sp) percentages, and area under the curve (AUROC) values.

Profile		Training				Validation		
	$f(v_{i,j})$	0[a]	1[a]	(%)	Par.	(%)	0[a]	1[a]
IFPTML-MLPC 1:1-100-100-1:1	0[b]	352	222	77.4	Sp	56.8	134	102
	1[b]	118	405	61.3	Sn	77.4	53	182
	AUROC		0.694				0.671	
IFPTML-MLPC 1:1-100-100-100-1:1	0[b]	491	83	85.5	Sp	78.8	186	50
	1[b]	170	353	67.5	Sn	63.8	85	750
	AUROC		0.765				0.713	
IFPTML-MLPC 1:1-100-1100-100-1:1	0[b]	187	82	85.7	Sp	79.2	187	49
	1[b]	171	352	67.3	Sn	63.0	87	148
	AUROC		0.765				0.711	

[a] f(vi,j)pred = 0 or 1 predicted values, [b] f(vi,j)obs = 0 or 1 observed values.

After testing an IFPTML-MLPC model in which the number of neurons and layers comprising the network has been varied, we observe that, starting from the architecture of two hidden dense layers with 100 neurons each, the prediction performance does not significantly improve the results obtained with the IFPTML-DCT model. The results obtained with this type of neural network are somewhat better in terms of specificity, but there was no significant improvement. Therefore, a more complex Deep Learning ANNs with the same architecture (16:16-64-32-32-1:1 ReLU activation, ADAM optimizer, binary cross entropy classification, Figure 4) was developed, but in order to optimize the training the number of epochs and batch size were varied. The neural networks defined as IFPTML-DEEP-ANN are neural networks with hidden dense layers. This means that in all the hidden layers comprising the neural network, every neuron is connected to all the preceding and subsequent neurons.

 doi:10.20944/preprints202411.1644.v1

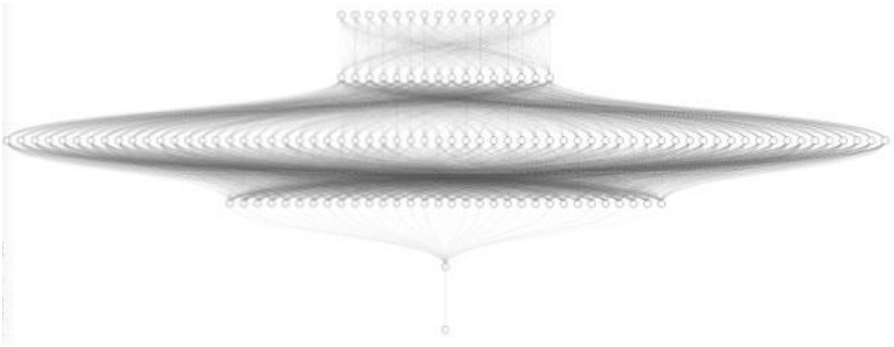

Figure 4. Architecture of the IFPTML-DEEP-ANN neural network with 16:16-64-32-32-32-1:1 configuration, showing the arrangement of layers and neurons for the model.

Various models were tested regarding different epochs and batch sizes. As shown in Table 6, the results do not improve in the same way across different batch sizes, although an improvement in results was observed as the number of epochs was increased. In the last IFPTML-DEEP-ANN case, where 1000 epochs were tested, better results were obtained, even competitive with the results of the previous linear models. As mentioned in other sections of this work, all these models are available in the web repository.

Table 6. Results of IFPTML-DEEP-ANN models trained with the 16:16-64-32-32-32-1:1 architecture, varying the number of epochs and batch sizes. Includes performance metrics for each configuration.

Epoch	Batch Size	Train				Test				
		Sp (%)	Sn (%)	Ac (%)	AUC	Sp (%)	Sn (%)	Ac (%)	AUC	Loss
100	32	66.9	80.1	73.2	0.832	61.8	82.6	72.2	0.783	0.611
	64	84.8	66.7	76.2	0.807	78.8	63	70.9	0.761	0.582
	128	60.8	78.2	69.1	0.818	56.7	78.3	67.5	0.774	0.61
200	32	79.4	74.6	77.1	0.861	73.7	73.6	73.7	0.792	0.596
	64	69.8	83.4	76.3	0.858	64.0	78.3	71.1	0.788	0.614
	128	83.0	69.8	76.6	0.856	76.3	66.8	71.5	0.789	0.602
500	32	86.6	68.6	78.3	0.895	78.4	66	72.2	0.815	0.656
1000	32	83.5	80.7	82.1	0.906	75.0	78.7	76.8	0.830	0.659
2000	32	79.4	81.2	80.3	0.915	72.5	80.0	76.2	0.815	0.886

To perform a visual analysis of the quality parameters of the model developed using the IFPTML-DEEP-ANN technique, Figure 5 shows the change in the loss value as a function of the number of epochs that have been trained.

 doi:10.20944/preprints202411.1644.v1

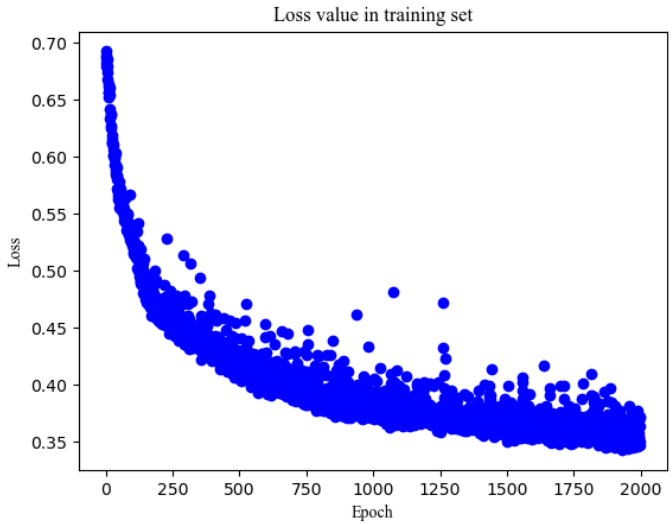

Figure 5. Evolution of the loss-value as a function of the number of epochs during model training.

4.2. Experimental and Computational Case of Study of ChiMA Gel

This case of study has two parts. Firstly, the experimental study of a set of bioprinted ChiMA scaffolds, and the analysis of the taken image. Afterwards, the results obtained with the predictive models will be shown.

4.2.1. Experimental Characterization of Two New ChiMA and ChiMA + PEGDA Hydrogel

Once a model was obtained to make the predictions (IFTPML-DTC), two hydrogel structures were printed to test the predictions made with the model and the actual results. The 3D printing of the ChiMA and ChiMA + PEGDA hydrogel inks was carried out as described in the corresponding section in the experimental part, obtaining the bioprinted designs shown in the Figure 6. With the photographs of the inks of the ChiMA (Figure 6A) and ChiMA + PEGDA (Figure 6B) the width, length, perimeter, and area of the hydrogel grids were obtained with the ImageJ software as previously described. These data were used to calculate the printability parameters of uniformity and expansion shown in Table 7.

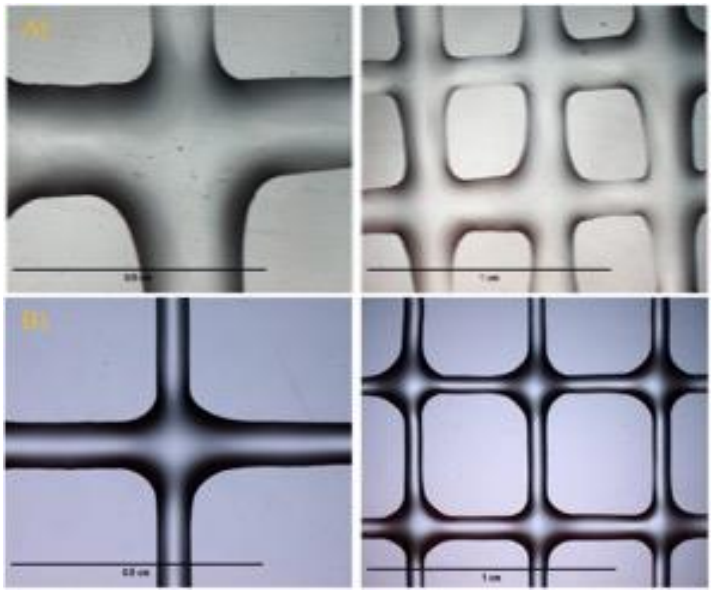

 doi:10.20944/preprints202411.1644.v1

Figure 6. A. ChiMA 3D printed scaffold. B. 3D printed scaffold by ChiMA + PEGDA. Both images show the structures of the bioprinted scaffolds, highlighting the differences in the composition and morphology of the materials used.

Table 7. Results obtained for ChiMA and ChiMA + PEGDA bioprint, including printing parameters, as well as observed and predicted classification using the model developed in this work.

	Parameter	Value	Classification Observed	Classification Predicted
ChiMA	Uniformity	0.94	1	1
	Expansion	6.44	0	0
	Porosity	0.38	0	0
ChiMA + PEGDA	Uniformity	0.98	1	0
	Expansion	2.78	0	0
	Porosity	0.69	0	0

The results obtained from the image analysis and the model can be assumed to be as expected. The model has been trained with a database in which most of the inputs were composed of a single hydrogel, that's why it was more accurate in making predictions of those experiments that best fit the training data.

4.2.2. IFPTML Computational Simulation of ChiMA Gel

In the previous sections we described the synthesis and analysis study of this pure ChiMA hydrogel 3D bioprinting assays. Even so, there are several unmeasured properties and conditions that can be predicted using the model. In order to visualise the predictions made by the model in a simpler way, a heatmap has been generated, which can be seen in Table 8. In this table, the values of the two main bioprinting conditions are changed: c_1 = Extrusion Pressure (kPa), c_2 = Extrusion speed (mm/s). In the table, the probability of classification as good (1) for each of the trials has been calculated while maintaining the rest of the conditions*. To make the visualisation of the values easier, the values from 0 to 1 have been coloured with a red-orange-green colour scale. In addition to the experimentally measured printing properties, the value of Integrity factor is predicted. The results can be seen in the heat-map in Table 8.

Table 8. Prediction heat map for ChiMA 1.5 w/v%, showing the probabilities of properties reaching desirable values when setting conditions and varying the values of c_1 and c_2.

		Extrusion speed (mm/s) (c_2)				Property
		1	7	10	25	
Extrusion P (kPa) (c_1)	25	0.071	0.927	0.071	0.148	Expansion
	30	0.583	0.148	0.583	0.071	
	35	0.148	0.071	0.148	0.927	
	48	0.071	0.927	0.071	0.148	
	25	0.071	0.927	0.071	0.148	Pr
	30	0.583	0.148	0.583	0.071	
	35	0.148	0.071	0.148	0.927	
	48	0.071	0.927	0.071	0.148	
	25	0.927	0.148	0.927	0.071	U
	30	0.148	0.071	0.148	0.583	
	35	0.071	0.927	0.071	0.148	
	48	0.927	0.148	0.927	0.071	
	25	0.071	0.927	0.071	1.000	I
	30	0.583	1.000	0.583	0.071	

 doi:10.20944/preprints202411.1644.v1

	35	1.000	0.071	1.000	0.927
	48	0.071	0.927	0.071	1.000
Color-scale for probability values		Low		Medium	High

*c_3 = 25G, c_4 = 254 μm, c_5 = 1, c_6 = 25ºC, c_7 = 25ºC, c_8 = 25ºC, c_9 = N,.

The results obtained in the experimental test and in the predictions, although are not equal, can be understood to be very close to reality. This may be because the margins for classification are very strict and those impressions that, although below, are close to the limits, can be considered a good result.

5. Conclusions

In this research, the starting point was the creation of a database created from scratch based on bibliography and tests carried out in the Labquimac research group of the UPV/EHU. In addition, the use of a model based on IFPTML for the processing of complex databases was demonstrated. The non-linear models developed showed better results than linear models and neural networks. Moreover, the model has been tested to understand the use of the models in a real case.

Author Contributions: Conceptualization, J.L.V.V and I.M.B; Methodology, H.B.B., M.N.D.S.C., A.K.H., H.G.D. and S.A.G.; Code, H.B.B.; Validation, H.B.B., S.A. and H.G.D.; Formal Analysis, S.A. and I.M.B.; Investigation, H.B.B.; Data Curation, H.B.B., M.N.D.S.C. and A.K.H.; Writing – Original Draft Preparation, H.B.B., S.A. and H.G.D.; Writing – Review & Editing, I.M.B.; Supervision, J.L.V.V.; Project Administration, J.L.V.V.; Funding Acquisition, J.L.V.V.

Funding: The authors acknowledge financial support from Basque Government SPRI ELKARTEK program grant (KK-2022/00057). AKH and MNDSC also acknowledge the financial support from Fundação para a Ciência e a Tecnologia (FCT/MCTES) through national funds (LAQV-REQUIMTE, grant UID/QUI/50006/2020). Authors are thankful for funding from the Government of the Basque Country under the Grupos de Investigación del Sistema Universitario Vasco (IT1756-22) program.

Data Availability Statement: Lastly, this section includes a link to the repository of the article, where the initial database and all the code generated during this research is located, thus ensuring transparency and clarity. In addition, the source code of the new methods is available through a publicly accessible service and is distributed under an open-source license. https://github.com/hbediaga/hydrogel (accessed on 4 November 2024).

Conflicts of Interest: The authors declare no conflicts of interest.

References

1. Roche, C.D.; Brereton, R.J.L.; Ashton, A.W.; Jackson, C.; Gentile, C. Current challenges in three-dimensional bioprinting heart tissues for cardiac surgery. *European Journal of Cardio-Thoracic Surgery* **2020**, *58*, 500-510, doi:10.1093/ejcts/ezaa093.
2. Unagolla, J.M.; Jayasuriya, A.C. Hydrogel-based 3D bioprinting: A comprehensive review on cell-laden hydrogels, bioink formulations, and future perspectives. *Applied Materials Today* **2020**, *18*, 100479, doi:https://doi.org/10.1016/j.apmt.2019.100479.
3. Chimene, D.; Lennox, K.K.; Kaunas, R.R.; Gaharwar, A.K. Advanced Bioinks for 3D Printing: A Materials Science Perspective. *Annals of Biomedical Engineering* **2016**, *44*, 2090-2102, doi:10.1007/s10439-016-1638-y.
4. Shah, P.P.; Shah, H.B.; Maniar, K.K.; Özel, T. Extrusion-based 3D bioprinting of alginate-based tissue constructs. *Procedia CIRP* **2020**, *95*, 143-148, doi:https://doi.org/10.1016/j.procir.2020.06.007.
5. Huang, J.; Lei, X.; Huang, Z.; Rong, Z.; Li, H.; Xie, Y.; Duan, L.; Xiong, J.; Wang, D.; Zhu, S.; et al. Bioprinted Gelatin-Recombinant Type III Collagen Hydrogel Promotes Wound Healing. *Int J Bioprint* **2022**, *8*, 517, doi:10.18063/ijb.v8i2.517.
6. Ding, Y.-W.; Zhang, X.-W.; Mi, C.-H.; Qi, X.-Y.; Zhou, J.; Wei, D.-X. Recent advances in hyaluronic acid-based hydrogels for 3D bioprinting in tissue engineering applications. *Smart Materials in Medicine* **2023**, *4*, 59-68, doi:https://doi.org/10.1016/j.smaim.2022.07.003.
7. Piluso, S.; Skvortsov, G.A.; Altunbek, M.; Afghah, F.; Khani, N.; Koç, B.; Patterson, J. 3D bioprinting of molecularly engineered PEG-based hydrogels utilizing gelatin fragments. *Biofabrication* **2021**, *13*, doi:10.1088/1758-5090/ac0ff0.
8. Rosińska, K.; Bartniak, M.; Wierzbicka, A.; Sobczyk-Guzenda, A.; Bociaga, D. Solvent types used for the preparation of hydrogels determine their mechanical properties and influence cell viability through

gelatine and calcium ions release. *J Biomed Mater Res B Appl Biomater* **2023**, *111*, 314-330, doi:10.1002/jbm.b.35152.

9. Darmau, B.; Hoang, A.; Gross, A.J.; Texier, I. Water-based synthesis of dextran-methacrylate and its use to design hydrogels for biomedical applications. *European Polymer Journal* **2024**, *221*, 113515, doi:https://doi.org/10.1016/j.eurpolymj.2024.113515.
10. Shamma, R.N.; Sayed, R.H.; Madry, H.; El Sayed, N.S.; Cucchiarini, M. Triblock Copolymer Bioinks in Hydrogel Three-Dimensional Printing for Regenerative Medicine: A Focus on Pluronic F127. *Tissue Engineering Part B: Reviews* **2021**, *28*, 451-463, doi:10.1089/ten.teb.2021.0026.
11. Wang, M.; Bai, J.; Shao, K.; Tang, W.; Zhao, X.; Lin, D.; Huang, S.; Chen, C.; Ding, Z.; Ye, J. Poly(vinyl alcohol) Hydrogels: The Old and New Functional Materials. *International Journal of Polymer Science* **2021**, *2021*, 2225426, doi:https://doi.org/10.1155/2021/2225426.
12. Ye, J.; Qian, C.; Dong, Y.; Zhu, Y.; Fu, Y. Development of organic solvent-induced shape memory poly(ethylene-co-vinyl acetate) monoliths for expandable oil absorbers. *European Polymer Journal* **2023**, *183*, 111730, doi:https://doi.org/10.1016/j.eurpolymj.2022.111730.
13. Dwivedi, R.; Kumar, S.; Pandey, R.; Mahajan, A.; Nandana, D.; Katti, D.S.; Mehrotra, D. Polycaprolactone as biomaterial for bone scaffolds: Review of literature. *J Oral Biol Craniofac Res* **2020**, *10*, 381-388, doi:10.1016/j.jobcr.2019.10.003.
14. Rodríguez-Rego, J.M.; Mendoza-Cerezo, L.; Macías-García, A.; Mendoza-Cerezo, L.; Carrasco-Amador, J.P.; Marcos-Romero, A.C. Methodology for characterizing the printability of hydrogels. *Int J Bioprint* **2023**, *9*, 667, doi:10.18063/ijb.v9i2.667.
15. Dell, A.C.; Wagner, G.; Own, J.; Geibel, J.P. 3D Bioprinting Using Hydrogels: Cell Inks and Tissue Engineering Applications. *Pharmaceutics* **2022**, *14*, doi:10.3390/pharmaceutics14122596.
16. Kaliaraj, G.S.; Shanmugam, D.K.; Dasan, A.; Mosas, K.K. Hydrogels—A Promising Materials for 3D Printing Technology. *Gels* **2023**, *9*, doi:10.3390/gels9030260.
17. Martin, T.B.; Audus, D.J. Emerging Trends in Machine Learning: A Polymer Perspective. *ACS Polymers Au* **2023**, *3*, 239-258, doi:10.1021/acspolymersau.2c00053.
18. Naghieh, S.; Chen, X. Printability–A key issue in extrusion-based bioprinting. *Journal of Pharmaceutical Analysis* **2021**, *11*, 564-579, doi:https://doi.org/10.1016/j.jpha.2021.02.001.
19. Zhang, T.; Zhao, W.; Zijie, X.H.; Wang, X.W.; Zhang, K.X.; Yin, J.B. Bioink design for extrusion-based bioprinting. *APPLIED MATERIALS TODAY* **2021**, *25*, doi:10.1016/j.apmt.2021.101227.
20. He, Y.; Yang, F.; Zhao, H.; Gao, Q.; Xia, B.; Fu, J. Research on the printability of hydrogels in 3D bioprinting. *Scientific Reports* **2016**, *6*, 29977, doi:10.1038/srep29977.
21. Lai, J.; Ye, X.; Liu, J.; Wang, C.; Li, J.; Wang, X.; Ma, M.; Wang, M. 4D printing of highly printable and shape morphing hydrogels composed of alginate and methylcellulose. *Materials & Design* **2021**, *205*, 109699, doi:https://doi.org/10.1016/j.matdes.2021.109699.
22. Jin, W.; Liu, H.; Li, Z.; Nie, P.; Zhao, G.; Cheng, X.; Zheng, G.; Yang, X. Effect of Hydrogel Contact Angle on Wall Thickness of Artificial Blood Vessel. *International Journal of Molecular Sciences* **2022**, *23*, doi:10.3390/ijms231911114.
23. Mancha Sánchez, E.; Gómez-Blanco, J.C.; López Nieto, E.; Casado, J.G.; Macías-García, A.; Díaz Díez, M.A.; Carrasco-Amador, J.P.; Torrejón Martín, D.; Sánchez-Margallo, F.M.; Pagador, J.B. Hydrogels for Bioprinting: A Systematic Review of Hydrogels Synthesis, Bioprinting Parameters, and Bioprinted Structures Behavior. *Frontiers in Bioengineering and Biotechnology* **2020**, *8*, doi:10.3389/fbioe.2020.00776.
24. Sällström, N.; Goulas, A.; Martin, S.; Engstrøm, D.S. The effect of print speed and material aging on the mechanical properties of a self-healing nanocomposite hydrogel. *Additive Manufacturing* **2020**, *35*, 101253, doi:https://doi.org/10.1016/j.addma.2020.101253.
25. Strauß, S.; Schroth, B.; Hubbuch, J. Evaluation of the Reproducibility and Robustness of Extrusion-Based Bioprinting Processes Applying a Flow Sensor. *Front Bioeng Biotechnol* **2022**, *10*, 831350, doi:10.3389/fbioe.2022.831350.
26. Lee, U.N.; Day, J.H.; Haack, A.J.; Bretherton, R.C.; Lu, W.; DeForest, C.A.; Theberge, A.B.; Berthier, E. Layer-by-layer fabrication of 3D hydrogel structures using open microfluidics. *Lab Chip* **2020**, *20*, 525-536, doi:10.1039/c9lc00621d.
27. Göhl, J.; Markstedt, K.; Mark, A.; Håkansson, K.; Gatenholm, P.; Edelvik, F. Simulations of 3D bioprinting: predicting bioprintability of nanofibrillar inks. *Biofabrication* **2018**, *10*, 034105, doi:10.1088/1758-5090/aac872.
28. GhavamiNejad, A.; Ashammakhi, N.; Wu, X.Y.; Khademhosseini, A. Crosslinking Strategies for 3D Bioprinting of Polymeric Hydrogels. *Small* **2020**, *16*, 2002931, doi:https://doi.org/10.1002/smll.202002931.
29. Xie, S. Perspectives on development of biomedical polymer materials in artificial intelligence age. *Journal of Biomaterials Applications* **2023**, *37*, 1355-1375, doi:10.1177/08853282231151822.
30. Hulsen, T. Literature analysis of artificial intelligence in biomedicine. *Ann Transl Med* **2022**, *10*, 1284, doi:10.21037/atm-2022-50.

31. Mazón-Ortiz, G.; Cerda-Mejía, G.; Gutiérrez Morales, E.; Diéguez-Santana, K.; Ruso, J.M.; González-Díaz, H. Trends in Nanoparticles for Leishmania Treatment: A Bibliometric and Network Analysis. *Diseases* **2023**, *11*, doi:10.3390/diseases11040153.
32. Nocedo-Mena, D.; Cornelio, C.; Camacho-Corona, M.D.R.; Garza-González, E.; Waksman de Torres, N.; Arrasate, S.; Sotomayor, N.; Lete, E.; González-Díaz, H. Modeling Antibacterial Activity with Machine Learning and Fusion of Chemical Structure Information with Microorganism Metabolic Networks. *J Chem Inf Model* **2019**, *59*, 1109-1120, doi:10.1021/acs.jcim.9b00034.
33. Quevedo-Tumailli, V.; Ortega-Tenezaca, B.; González-Díaz, H. IFPTML Mapping of Drug Graphs with Protein and Chromosome Structural Networks vs. Pre-Clinical Assay Information for Discovery of Antimalarial Compounds. *International Journal of Molecular Sciences* **2021**, *22*, doi:10.3390/ijms222313066.
34. Santana, R.; Zuluaga, R.; Gañán, P.; Arrasate, S.; Onieva Caracuel, E.; González-Díaz, H. PTML Model of ChEMBL Compounds Assays for Vitamin Derivatives. *ACS Combinatorial Science* **2020**, *22*, 129-141, doi:10.1021/acscombsci.9b00166.
35. Santiago, C.; Ortega-Tenezaca, B.; Barbolla, I.; Fundora-Ortiz, B.; Arrasate, S.; Dea-Ayuela, M.A.; González-Díaz, H.; Sotomayor, N.; Lete, E. Prediction of Antileishmanial Compounds: General Model, Preparation, and Evaluation of 2-Acylpyrrole Derivatives. *Journal of Chemical Information and Modeling* **2022**, *62*, 3928-3940, doi:10.1021/acs.jcim.2c00731.
36. Helguera, A.M.; Combes, R.D.; González, M.P.; Cordeiro, M.N. Applications of 2D descriptors in drug design: a DRAGON tale. *Curr Top Med Chem* **2008**, *8*, 1628-1655, doi:10.2174/156802608786786598.
37. Leini, Z.; Xiaolei, S. Study on Speech Recognition Method of Artificial Intelligence Deep Learning. *Journal of Physics: Conference Series* **2021**, *1754*, 012183, doi:10.1088/1742-6596/1754/1/012183.
38. Ennaji, O.; Vergütz, L.; El Allali, A. Machine learning in nutrient management: A review. *Artificial Intelligence in Agriculture* **2023**, *9*, 1-11, doi:https://doi.org/10.1016/j.aiia.2023.06.001.
39. Kakani, V.; Nguyen, V.H.; Kumar, B.P.; Kim, H.; Pasupuleti, V.R. A critical review on computer vision and artificial intelligence in food industry. *Journal of Agriculture and Food Research* **2020**, *2*, 100033, doi:https://doi.org/10.1016/j.jafr.2020.100033.
40. Barreiro, E.; Munteanu, C.R.; Cruz-Monteagudo, M.; Pazos, A.; González-Díaz, H. Net-Net Auto Machine Learning (AutoML) Prediction of Complex Ecosystems. *Sci Rep* **2018**, *8*, 12340, doi:10.1038/s41598-018-30637-w.
41. Madadian Bozorg, N.; Leclercq, M.; Lescot, T.; Bazin, M.; Gaudreault, N.; Dikpati, A.; Fortin, M.-A.; Droit, A.; Bertrand, N. Design of experiment and machine learning inform on the 3D printing of hydrogels for biomedical applications. *Biomaterials Advances* **2023**, *153*, 213533, doi:https://doi.org/10.1016/j.bioadv.2023.213533.
42. Yang, B.; Zhao, Y.; Wei, Y.; Fu, C.; Tao, L. The Ugi reaction in polymer chemistry: syntheses, applications and perspectives. *Polymer Chemistry* **2015**, *6*, 8233-8239, doi:10.1039/C5PY01398D.
43. Li, F.; Han, J.; Cao, T.; Lam, W.; Fan, B.; Tang, W.; Chen, S.; Fok, K.L.; Li, L. Design of self-assembly dipeptide hydrogels and machine learning via their chemical features. *Proceedings of the National Academy of Sciences* **2019**, *116*, 11259-11264, doi:10.1073/pnas.1903376116.
44. Yadav, D.; Chhabra, D.; Kumar Garg, R.; Ahlawat, A.; Phogat, A. Optimization of FDM 3D printing process parameters for multi-material using artificial neural network. *Materials Today: Proceedings* **2020**, *21*, 1583-1591, doi:https://doi.org/10.1016/j.matpr.2019.11.225.
45. Elbadawi, M.; Muñiz Castro, B.; Gavins, F.K.H.; Ong, J.J.; Gaisford, S.; Pérez, G.; Basit, A.W.; Cabalar, P.; Goyanes, A. M3DISEEN: A novel machine learning approach for predicting the 3D printability of medicines. *Int J Pharm* **2020**, *590*, 119837, doi:10.1016/j.ijpharm.2020.119837.
46. Nadernezhad, A.; Groll, J. Machine Learning Reveals a General Understanding of Printability in Formulations Based on Rheology Additives. *Advanced Science* **2022**, *9*, 2202638, doi:https://doi.org/10.1002/advs.202202638.
47. Chen, H.; Liu, Y.; Balabani, S.; Hirayama, R.; Huang, J. Machine Learning in Predicting Printable Biomaterial Formulations for Direct Ink Writing. *Research 6*, 0197, doi:10.34133/research.0197.
48. Bediaga, H.; Moreno, M.I.; Arrasate, S.; Vilas, J.L.; Orbe, L.; Unzueta, E.; Mercader, J.P.; González-Díaz, H. Multi-output chemometrics model for gasoline compounding. *Fuel* **2022**, *310*, 122274, doi:https://doi.org/10.1016/j.fuel.2021.122274.
49. Cabrera-Andrade, A.; López-Cortés, A.; Munteanu, C.R.; Pazos, A.; Pérez-Castillo, Y.; Tejera, E.; Arrasate, S.; González-Díaz, H. Perturbation-Theory Machine Learning (PTML) Multilabel Model of the ChEMBL Dataset of Preclinical Assays for Antisarcoma Compounds. *ACS Omega* **2020**, *5*, 27211-27220, doi:10.1021/acsomega.0c03356.
50. Aranzamendi, E.; Arrasate, S.; Sotomayor, N.; González-Díaz, H.; Lete, E. Chiral Brønsted Acid-Catalyzed Enantioselective α-Amidoalkylation Reactions: A Joint Experimental and Predictive Study. *ChemistryOpen* **2016**, *5*, 540-549, doi:10.1002/open.201600120.
51. Blay, V.; Yokoi, T.; González-Díaz, H. Perturbation Theory–Machine Learning Study of Zeolite Materials Desilication. *Journal of Chemical Information and Modeling* **2018**, *58*, 2414-2419, doi:10.1021/acs.jcim.8b00383.

52. Carracedo-Reboredo, P.; Aranzamendi, E.; He, S.; Arrasate, S.; Munteanu, C.; Fernandez-Lozano, C.; Sotomayor, N.; Lete, E.; González-Díaz, H. MATEO: InterMolecular α-Amidoalkylation Theoretical Enantioselectivity Optimization. Online Tool for Selection and Design of Chiral Catalysts and Products. **2023**, doi:10.21203/rs.3.rs-2642502/v1.
53. Concu, R.; MN, D.S.C.; Munteanu, C.R.; González-Díaz, H. PTML Model of Enzyme Subclasses for Mining the Proteome of Biofuel Producing Microorganisms. *J Proteome Res* **2019**, *18*, 2735-2746, doi:10.1021/acs.jproteome.8b00949.
54. Correa Gonzalez, S.; Kroyan, Y.; Sarjovaara, T.; Kiiski, U.; Karvo, A.; Toldy, A.I.; Larmi, M.; Santasalo-Aarnio, A. Prediction of Gasoline Blend Ignition Characteristics Using Machine Learning Models. *Energy & Fuels* **2021**, *35*, 9332-9340, doi:10.1021/acs.energyfuels.1c00749.
55. Ewald, J.; Jansen, P.M.; Brunke, S.; Hiller, D.; Luther, C.; González-Díaz, H.; Dittrich, M.; Fleißner, A.; Hube, B.; Schuster, S.; et al. The landscape of toxic intermediates in the metabolic networks of pathogenic fungi reveals targets for antifungal drugs. **2021**, doi:10.1101/2021.09.05.459012.
56. Quevedo-Tumailli, V.F.; Ortega-Tenezaca, B.; González-Díaz, H. Chromosome Gene Orientation Inversion Networks (GOINs) of Plasmodium Proteome. *J Proteome Res* **2018**, *17*, 1258-1268, doi:10.1021/acs.jproteome.7b00861.
57. Liu, Z.; Xin, W.; Ji, J.; Xu, J.; Zheng, L.; Qu, X.; Yue, B. 3D-Printed Hydrogels in Orthopedics: Developments, Limitations, and Perspectives. *Frontiers in Bioengineering and Biotechnology* **2022**, *10*, doi:10.3389/fbioe.2022.845342.
58. Aguado, B.A.; Mulyasasmita, W.; Su, J.; Lampe, K.J.; Heilshorn, S.C. Improving viability of stem cells during syringe needle flow through the design of hydrogel cell carriers. *Tissue Eng Part A* **2012**, *18*, 806-815, doi:10.1089/ten.TEA.2011.0391.
59. Almeida, C.R.; Serra, T.; Oliveira, M.I.; Planell, J.A.; Barbosa, M.A.; Navarro, M. Impact of 3-D printed PLA- and chitosan-based scaffolds on human monocyte/macrophage responses: Unraveling the effect of 3-D structures on inflammation. *Acta Biomaterialia* **2014**, *10*, 613-622, doi:https://doi.org/10.1016/j.actbio.2013.10.035.
60. Butler, H.M.; Naseri, E.; MacDonald, D.S.; Tasker, R.A.; Ahmadi, A. Investigation of rheology, printability, and biocompatibility of N,O-carboxymethyl chitosan and agarose bioinks for 3D bioprinting of neuron cells. *Materialia* **2021**, *18*, 101169, doi:https://doi.org/10.1016/j.mtla.2021.101169.
61. Chen, Y.; Xiong, X.; Liu, X.; Cui, R.; Wang, C.; Zhao, G.; Zhi, W.; Lu, M.; Duan, K.; Weng, J.; et al. 3D Bioprinting of shear-thinning hybrid bioinks with excellent bioactivity derived from gellan/alginate and thixotropic magnesium phosphate-based gels. *Journal of Materials Chemistry B* **2020**, *8*, 5500-5514, doi:10.1039/D0TB00060D.
62. Contessi Negrini, N.; Bonetti, L.; Contili, L.; Farè, S. 3D printing of methylcellulose-based hydrogels. *Bioprinting* **2018**, *10*, e00024, doi:https://doi.org/10.1016/j.bprint.2018.e00024.
63. Firipis, K.; Footner, E.; Boyd-Moss, M.; Dekiwadia, C.; Nisbet, D.; Kapsa, R.M.I.; Pirogova, E.; Williams, R.J.; Quigley, A. Biodesigned bioinks for 3D printing via divalent crosslinking of self-assembled peptide-polysaccharide hybrids. *Materials Today Advances* **2022**, *14*, 100243, doi:https://doi.org/10.1016/j.mtadv.2022.100243.
64. Gao, H.; Zhang, W.; Yu, Z.; Xin, F.; Jiang, M. Emerging Applications of 3D Printing in Biomanufacturing. *Trends in Biotechnology* **2021**, *39*, 1114-1116, doi:https://doi.org/10.1016/j.tibtech.2021.04.005.
65. Giuseppe, M.D.; Law, N.; Webb, B.; A. Macrae, R.; Liew, L.J.; Sercombe, T.B.; Dilley, R.J.; Doyle, B.J. Mechanical behaviour of alginate-gelatin hydrogels for 3D bioprinting. *Journal of the Mechanical Behavior of Biomedical Materials* **2018**, *79*, 150-157, doi:https://doi.org/10.1016/j.jmbbm.2017.12.018.
66. Jain, T.; Baker, H.B.; Gipsov, A.; Fisher, J.P.; Joy, A.; Kaplan, D.S.; Isayeva, I. Impact of cell density on the bioprinting of gelatin methacrylate (GelMA) bioinks. *Bioprinting* **2021**, *22*, e00131, doi:https://doi.org/10.1016/j.bprint.2021.e00131.
67. Ouyang, L.; Yao, R.; Zhao, Y.; Sun, W. Effect of bioink properties on printability and cell viability for 3D bioplotting of embryonic stem cells. *Biofabrication* **2016**, *8*, doi:10.1088/1758-5090/8/3/035020.
68. Maiz-Fernández, S.; Pérez-Álvarez, L.; Silván, U.; Vilas-Vilela, J.L.; Lanceros-Méndez, S. Dynamic and Self-Healable Chitosan/Hyaluronic Acid-Based In Situ-Forming Hydrogels. *Gels* **2022**, *8*, doi:10.3390/gels8080477.
69. Gao, T.; Gillispie, G.J.; Copus, J.S.; Pr, A.K.; Seol, Y.-J.; Atala, A.; Yoo, J.J.; Lee, S.J. Optimization of gelatin-alginate composite bioink printability using rheological parameters: a systematic approach. *Biofabrication* **2018**, *10*, 034106-034106, doi:10.1088/1758-5090/aacdc7.
70. Soltan, N.; Ning, L.; Mohabatpour, F.; Papagerakis, P.; Chen, X. Printability and Cell Viability in Bioprinting Alginate Dialdehyde-Gelatin Scaffolds. *ACS Biomaterials Science & Engineering* **2019**, *5*, 2976-2987, doi:10.1021/acsbiomaterials.9b00167.
71. Weininger, D. SMILES, a chemical language and information system. 1. Introduction to methodology and encoding rules. *Journal of Chemical Information and Computer Sciences* **1988**, *28*, 31-36, doi:10.1021/ci00057a005.

72. van Rossum, G. Python reference manual. **1995**.
73. Moriwaki, H.; Tian, Y.-S.; Kawashita, N.; Takagi, T. Mordred: a molecular descriptor calculator. *Journal of Cheminformatics* **2018**, *10*, 4, doi:10.1186/s13321-018-0258-y.
74. Mauri, A. alvaDesc: A Tool to Calculate and Analyze Molecular Descriptors and Fingerprints. In *Ecotoxicological QSARs*, Roy, K., Ed.; Springer US: New York, NY, 2020; pp. 801-820.
75. Fattah, J.; Ezzine, L.; Aman, Z.; El Moussami, H.; Lachhab, A. Forecasting of demand using ARIMA model. *International Journal of Engineering Business Management* **2018**, *10*, 1847979018808673, doi:10.1177/1847979018808673.
76. Boland, J. Box–Jenkins Time Series Models. In *International Encyclopedia of Statistical Science*, Lovric, M., Ed.; Springer Berlin Heidelberg: Berlin, Heidelberg, 2011; pp. 178-181.
77. Schindelin, J.; Arganda-Carreras, I.; Frise, E.; Kaynig, V.; Longair, M.; Pietzsch, T.; Preibisch, S.; Rueden, C.; Saalfeld, S.; Schmid, B.; et al. Fiji: an open-source platform for biological-image analysis. *Nat Methods* **2012**, *9*, 676-682, doi:10.1038/nmeth.2019.
78. Boedeker, P.; Kearns, N.T. Linear Discriminant Analysis for Prediction of Group Membership: A User-Friendly Primer. *Advances in Methods and Practices in Psychological Science* **2019**, *2*, 250-263, doi:10.1177/2515245919849378.
79. Chen, X.w.; Jeong, J.C. Enhanced recursive feature elimination. In Proceedings of the Sixth International Conference on Machine Learning and Applications (ICMLA 2007), 13-15 Dec. 2007, 2007; pp. 429-435.
80. Xu, K.; Das, K.C. On Harary index of graphs. *Discrete Applied Mathematics* **2011**, *159*, 1631-1640, doi:https://doi.org/10.1016/j.dam.2011.06.003.
81. Schrier, J. Can One Hear the Shape of a Molecule (from its Coulomb Matrix Eigenvalues)? *Journal of Chemical Information and Modeling* **2020**, *60*, 3804-3811, doi:10.1021/acs.jcim.0c00631.
82. Ivanciuc, O. QSAR Comparative Study of Wiener Descriptors for Weighted Molecular Graphs. *Journal of Chemical Information and Computer Sciences* **2000**, *40*, 1412-1422, doi:10.1021/ci000068y.
83. Kavithaa, S.; Kaladevi, V. Gutman Index and Detour Gutman Index of Pseudo-Regular Graphs. *Journal of Applied Mathematics* **2017**, *2017*, 4180650, doi:10.1155/2017/4180650.
84. Bonchev, D.; Markel, E.; Dekmezian, A. Topological Analysis of Long-Chain Branching Patterns in Polyolefins. *Journal of Chemical Information and Computer Sciences* **2001**, *41*, 1274-1285, doi:10.1021/ci010021s.
85. Lukovits, I. An All-Path Version of the Wiener Index. *Journal of Chemical Information and Computer Sciences* **1998**, *38*, 125-129, doi:10.1021/ci9700541.
86. Montavon, G.; Rupp, M.; Gobre, V.; Vazquez-Mayagoitia, A.; Hansen, K.; Tkatchenko, A.; Müller, K.-R.; Anatole von Lilienfeld, O. Machine learning of molecular electronic properties in chemical compound space. *New Journal of Physics* **2013**, *15*, 095003, doi:10.1088/1367-2630/15/9/095003.
87. Plavšić, D.; Nikolić, S.; Trinajstić, N.; Mihalić, Z. On the Harary index for the characterization of chemical graphs. *Journal of Mathematical Chemistry* **1993**, *12*, 235-250, doi:10.1007/BF01164638.
88. Hollas, B. An Analysis of the Autocorrelation Descriptor for Molecules. *Journal of Mathematical Chemistry* **2003**, *33*, 91-101, doi:10.1023/A:1023247831238.
89. Liu, X.; Zhan, Q. The Expected Values for the Gutman Index and Schultz Index in the Random Regular Polygonal Chains. *Molecules* **2022**, *27*, doi:10.3390/molecules27206838.
90. Developers, T. *TensorFlow*, v2.15.0-rc1; Zenodo: 2023.
91. Chollet, F.; Others. Keras. **2015**.